

Article

# NiFeO<sub>x</sub> and NiFeCoO<sub>x</sub> Catalysts for Anion Exchange Membrane Water Electrolysis

Khaja Wahab Ahmed <sup>\*</sup>, Myeong Je Jang, Saeed Habibpour , Zhongwei Chen and Michael Fowler <sup>\*</sup>

Department of Chemical Engineering, University of Waterloo, Waterloo, ON N2L 3G1, Canada

<sup>\*</sup> Correspondence: kwahmed@uwaterloo.ca (K.W.A.); mfowler@uwaterloo.ca (M.F.);

Tel.: +1-519-888-4567 (ext. 33415) (M.F.)

**Abstract:** Hydrogen production using an Anion exchange membrane (AEM) electrolyzer allows the use of non-platinum group metal catalysts for oxygen evolution reaction (OER). Nickel and Cobalt-based oxides are active in an alkaline environment for OER and are relatively inexpensive compared to IrO<sub>2</sub> catalysts used in Polymer electrolyte membrane (PEM) electrolysis. Mixed metal oxide catalysts NiFeO<sub>x</sub> and NiFeCoO<sub>x</sub> catalysts were synthesized by the coprecipitation method using NaOH. X-ray diffraction results showed mainly NiO diffraction peaks for the NiFeO<sub>x</sub> catalyst due to the low concentration of Fe, for the NiFeCoO<sub>x</sub> catalyst, NiCo<sub>2</sub>O<sub>4</sub> diffraction peaks were observed. NiFeCoO<sub>x</sub> catalysts showed a higher Anion exchange membrane water electrolysis (AEMWE) performance compared to NiFeO<sub>x</sub> and commercial NiO, the highest current density at 2 V was 802 mA cm<sup>-2</sup> at 70 °C using 1 M KOH as an electrolyte. The effect of electrolyte concentration was studied by using 0.01 M, 0.1 M and 1 M KOH concentrations in an electrolysis operation. Electrochemical Impedance spectroscopy was performed along with the equivalent circuit fitting to calculate ohmic and activation resistances, the results showed a decrease in ohmic and activation resistances with the increase in electrolyte concentration. Commercially available AEM (Fumasep FAA-3-50 and Sustainion dioxide membrane X-37-50 grade T) were tested at similar conditions and their performance was compared. EIS results showed that X-37-50 offered lower ohmic resistance than the FAA-3-50 membrane.

**Keywords:** AEM; OER; PEM; NiO; NiFeO<sub>x</sub>; NiFeCoO<sub>x</sub>; EIS; ohmic resistance



**Citation:** Ahmed, K.W.; Jang, M.J.; Habibpour, S.; Chen, Z.; Fowler, M. NiFeO<sub>x</sub> and NiFeCoO<sub>x</sub> Catalysts for Anion Exchange Membrane Water Electrolysis. *Electrochem* **2022**, *3*, 843–861. <https://doi.org/10.3390/electrochem3040055>

Academic Editor: Masato Sone

Received: 2 October 2022

Accepted: 6 December 2022

Published: 14 December 2022

**Publisher's Note:** MDPI stays neutral with regard to jurisdictional claims in published maps and institutional affiliations.



**Copyright:** © 2022 by the authors. Licensee MDPI, Basel, Switzerland. This article is an open access article distributed under the terms and conditions of the Creative Commons Attribution (CC BY) license (<https://creativecommons.org/licenses/by/4.0/>).

## 1. Introduction

AEM electrolyzers are a new generation of water electrolyzers with solid polymer electrolyte membranes replacing the diaphragm and are receiving much attention due to their several advantages, such as low ohmic resistance, good gas separation, and use of non-platinum group metal (PGM) catalysts [1]. The thin anion quaternary ammonium ion exchange membrane is used to conduct OH<sup>-</sup> ions, which is cheaper than the polymer electrolyte membrane (PEM) [2–4].

Anion exchange membrane water electrolysis (AEMWE) has the advantage of being able to operate in low concentrations of electrolytes, such as 1% KOH or distilled water compared to conventional Alkaline water electrolysis (AWE), which makes it possible to use inexpensive Ni and Co-based electrocatalysts [4,5]. It also reduces the accumulation of K<sub>2</sub>CO<sub>3</sub> precipitates by the reaction of KOH with CO<sub>2</sub> in the atmosphere. To improve the current density and efficiency of AEMWE, a cell structure similar to polymer electrolyte membrane water electrolysis (PEMWE) is available [6–9]. AEMWE using a zero-gap alkaline electrolysis cell has been reported to perform better than 3 A cm<sup>-2</sup> at 1.8 V using 1 M KOH [10,11].

For OER in alkaline conditions, the reaction involved the consumption of OH<sup>-</sup> ions at the anode. The OH<sup>-</sup> ions are transported through the membrane from the cathode side. The OER reaction is the main reaction in water electrolysis and has a higher overpotential than the HER [12]. The mechanism of oxygen evolution involves several intermediate steps,

and it is kinetically unfavorable due to the four-electrons process for the evolution of one molecule of oxygen gas. This resulted in the formation of energy barriers and cause slower kinetics and high overpotential [13]. Due to this, the development of active, stable, and cost-effective OER catalysts is necessary to achieve higher electrolysis efficiencies.

Several materials and different compositions have been used for the OER, in alkaline conditions, first-row transition metals showed high activity, in addition, they have good stability in alkaline environments [14]. Ni, Fe, and Co-based catalysts have been known to decrease the OER overpotential [8,15–17]. Transition metal oxides, hydroxides, and oxyhydroxides have been studied for the OER and their activities have been reported in the literature. The general trend in the activity for these catalysts is Ni > Co > Fe [18–21].

Nickel has been proposed to be the most efficient catalyst for OER based on adsorption energies and bond strength of the reaction intermediates [19–22]. To further improve the activity of Ni hydroxides and oxyhydroxides, other transition metals are incorporated in a small amount to enhance the activity of the catalyst. The incorporation of transition metals has been shown to significantly affect the electronic properties of the catalyst [23,24]. In theory, the addition of the transition metal to metal oxide or hydroxide, affects the d-d intermetallic bonding between the metallic phases, and it could result in lower intermediate adsorption energy of the intermediates in the reaction [25]. This results in weaker adsorption of the intermediates and faster kinetics of the reaction. The addition of transition metals as impurities into Nickel oxide is reported to improve the conductivity, increase the active sites, and decrease the binding energy of the intermediates. [26–28].

The performance of AEMWE is highly dependent on the AEM and concentration of electrolytes as well as the electrocatalysts [4]. In AEMWE, various electrolytes such as KOH,  $K_2CO_3$  and  $KHCO_3$  are used to improve the performance [4,29]. Higher concentrations of electrolyte generally ensure higher ionic conductivity of the  $OH^-$ , which can be expected to improve performance. However, DI water can also be used as an electrolyte to prevent the corrosion of components [30,31].

In this study, we compared three different OER catalysts NiO,  $NiFeO_x$ , and  $NiFeCoO_x$  for AEMWE. The effect of electrolytes was also studied by varying the concentration of KOH. Electrochemical impedance spectroscopy (EIS) was performed to investigate different resistances during the operation of the electrolyzer. In addition, two different membranes (Fumasep FAA-3-50 and Sustainion dioxide membrane X-37-50 grade T) were compared. EIS with the equivalent circuit fitting was performed to evaluate the reason for different performances under similar conditions. The catalyst performance for the electrolysis was in the order of  $NiFeCoO_x > NiFeO_x > NiO$ . Unlike other studies performed on these catalysts at lower current densities and in three-electrode systems, this work evaluated the catalyst at higher current densities in AEMWE. EIS was also measured at higher temperatures and at high current densities in AEM electrolysis which are not always included in AEM electrolysis literature.

## 2. Experimental

### 2.1. Synthesis of Catalyst

The  $NiFeCoO_x$  catalyst was synthesized by the coprecipitation method at room temperature.  $Ni(NO_3)_2 \cdot 6H_2O$ ,  $Co(NO_3)_2 \cdot 6H_2O$ , and  $Fe(NO_3)_3 \cdot 9H_2O$  were used as a precursor of Ni, Co, and Fe, respectively. The mole fraction of Ni, Co, and Fe were 0.648, 0.324, and 0.027, respectively. Precursors were dissolved in water and kept at 25 °C. The precipitation step was carried out by adding 1 M NaOH dropwise for 1 h until precipitation stops. After the precipitation, the suspension was stirred for 2 h, and the catalyst suspension was centrifuged to get the solid catalyst. The solids obtained after centrifuging were washed with plenty of water to remove excess NaOH. The solid obtained after washing was dried in an oven overnight and then calcined/annealed in the furnace at 300 °C for 5 h to convert the catalyst into oxide form.  $NiFeO_x$  catalyst was also developed by the same method with Ni and Fe mole fractions of 0.85 and 0.15. All the chemicals used in the synthesis were from Sigma Aldrich, Saint Louis, MI, USA.

## 2.2. Preparation of the Membrane Electrode Assembly

NiO, NiFeO<sub>x</sub>, and NiFeCoO<sub>x</sub> catalysts were deposited on the nickel foam (thickness 1.7 mm), which is used as the anode. The catalyst slurry was made by dispersing 100 mg of catalyst in water and Nafion solution (Nafion™ 1100 W from Sigma Aldrich), if the slurry is too thick, an additional amount of water was added dropwise using a micropipette to get the proper consistency, the Nafion content was 10 wt% of the catalyst amount. After making the slurry, it was sonicated for 30 min to make a uniform mix. The thick catalyst slurry was then pasted on the surface of nickel foam and hot pressed to get the catalyst-coated gas diffusion electrode (GDE). In all cases, the catalyst loading at the anode was 25 mg·cm<sup>-2</sup>. The final thickness of the electrode was 0.75 mm. Figure 1a,b shows nickel foam which is a gas diffusion layer (GDL) at the anode side and carbon paper coated with Pt/C catalyst which is used at the cathode side. Nickel foam coated with the catalyst and AEM on top of carbon paper is shown in Figure 1c,d. The dimensions of the GDLs are 1.8 cm × 1.8 cm. Figure 2a,b shows the Membrane electrode assembly (MEA) from the cathode side and anode side, with AEM sandwiched in between them.

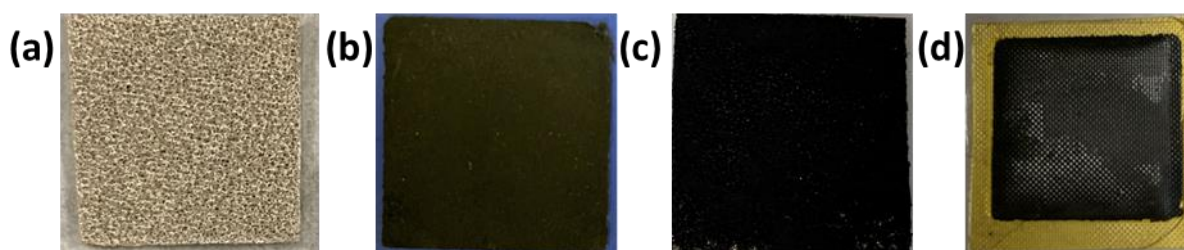


**Figure 1.** (a) Nickel foam (b) carbon paper coated with Pt/C catalyst, (c) Nickel foam anode coated with NiFeCoO<sub>x</sub> catalyst and (d) AEM with carbon paper cathode attached on one side. The dimensions of the electrodes were 1.8 cm × 1.8 cm.

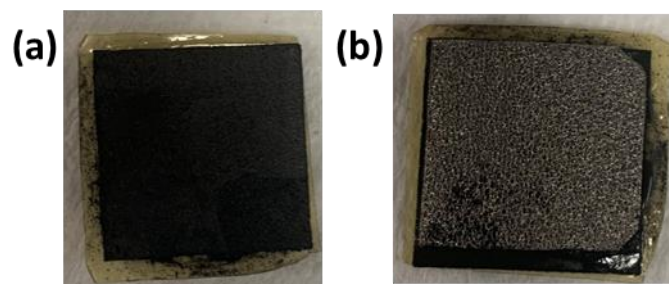


**Figure 2.** MEA after the electrolysis operation (a) MEA with cathode side (carbon paper) on top and (b) MEA with anode side (nickel foam) on top. The dimensions of the electrodes were 1.8 cm × 1.8 cm.

Commercial Pt/C (40 wt%, HISPEC 4000, Johnson Matthey, London, UK) catalyst was used for HER at the cathode, and 1 mg of Pt was deposited by drop casting method on the carbon paper (Sigracet 29BC) which has a thickness of 235 μm. The catalyst ink was prepared by adding the catalyst to water, ethanol, and a Nafion solution. For a typical ink composition, 50 mg of Pt/C was dispersed in 5 mL of ethanol and 1 mL of water with 0.22 g of Nafion solution. The Nafion content was 20 wt% of the catalyst amount. After the fabrication of the gas diffusion electrodes, the MEA was formed by adding AEM (Fumasep FAA-3-50 or dioxide membrane X-37-50 grade T) between the anode and cathode. The commercial AEM is in Cl or Br form, to use them in AEM electrolyzer, they are soaked in a 1.0 M KOH solution overnight (about 24 h) and rinsed with distilled water. The final activated membrane was used for the fabrication of MEA. The MEA was not pressed because it was possible to puncture the membrane due to the nickel foam. The MEA was formed by inserting the components in the MEA plastic casing, A porous transport layer made by pressing 3 nickel foams which were pressed to the thickness of 2 mm was first put

into the casing; then, a nickel foam anode is inserted in the casing followed by the AEM and then, the carbon paper cathode. The MEA was pressed during the tightening of the electrolyzer.

### 2.3. AEM Electrolyzer Single-Cell Tests

The performance of AEMWE was evaluated by using a potentiostat connected with 100 A Booster VMP3B-100. The AEM electrolyzer had a water inlet and water and oxygen outlet on the anode side and hydrogen outlet at the cathode side. The total active area of the MEA was 3.24 cm<sup>2</sup> with dimensions of 1.8 cm × 1.8 cm. The catalyst was activated by performing cyclic voltammetry (CV) in the range of 1.3 V to 2.2 V at a scan rate of 5 Mv·s<sup>-1</sup>. The operation was also performed by using linear sweep voltammetry (LSV) and chronoamperometry (CA). KOH was used as an electrolyte and was circulated with a flow rate of 90 mL/min. A hot plate was used to heat the electrolyte and the electrolyzer at the desired temperature, the temperature range used in electrolysis was from 45 to 70 °C.

EIS measurements were carried out to get the impedance of the electrolyzer cell during the operation. Potentiostatic EIS was performed at the voltage range of 1.7 V to 2 V, with a frequency range of 100 kHz to 100 mHz, the data were analyzed by Nyquist curves and further equivalent circuit fitting.

Half-cell reactions at the anode and cathode are shown in Equations (1) and (2), the overall reaction in AEM electrolyzer is shown in Equation (3). The theoretical voltage required to split water is 1.23 V, in practical cases, it is higher than 1.23 V due to the overpotential of these reactions at the anode and cathode.

Figure 3 shows a schematic of the AEM electrolyzer, in which the anode and cathode are separated by a thin polymeric AEM. In this work, the KOH aqueous solution is circulated from the anode side only. The reduction of water takes place at the cathode to form hydrogen, the OH<sup>-</sup> transports through the AEM and oxidized to give O<sub>2</sub> at the anode.

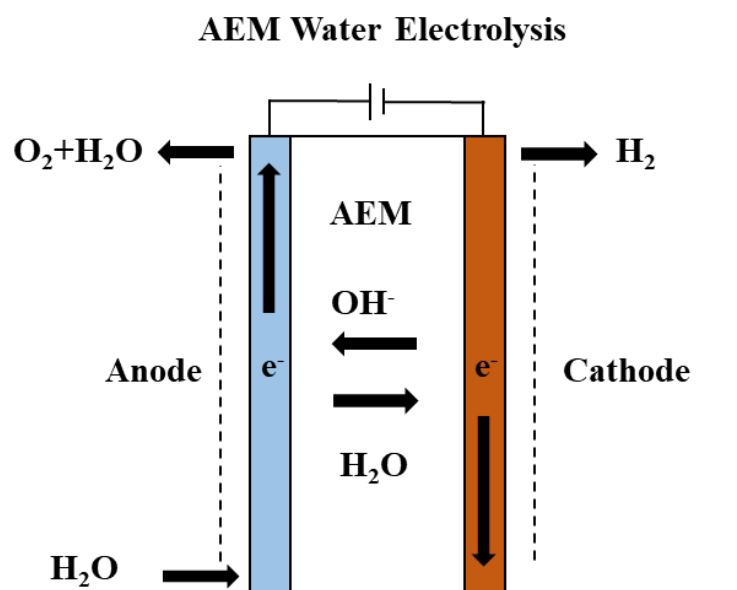
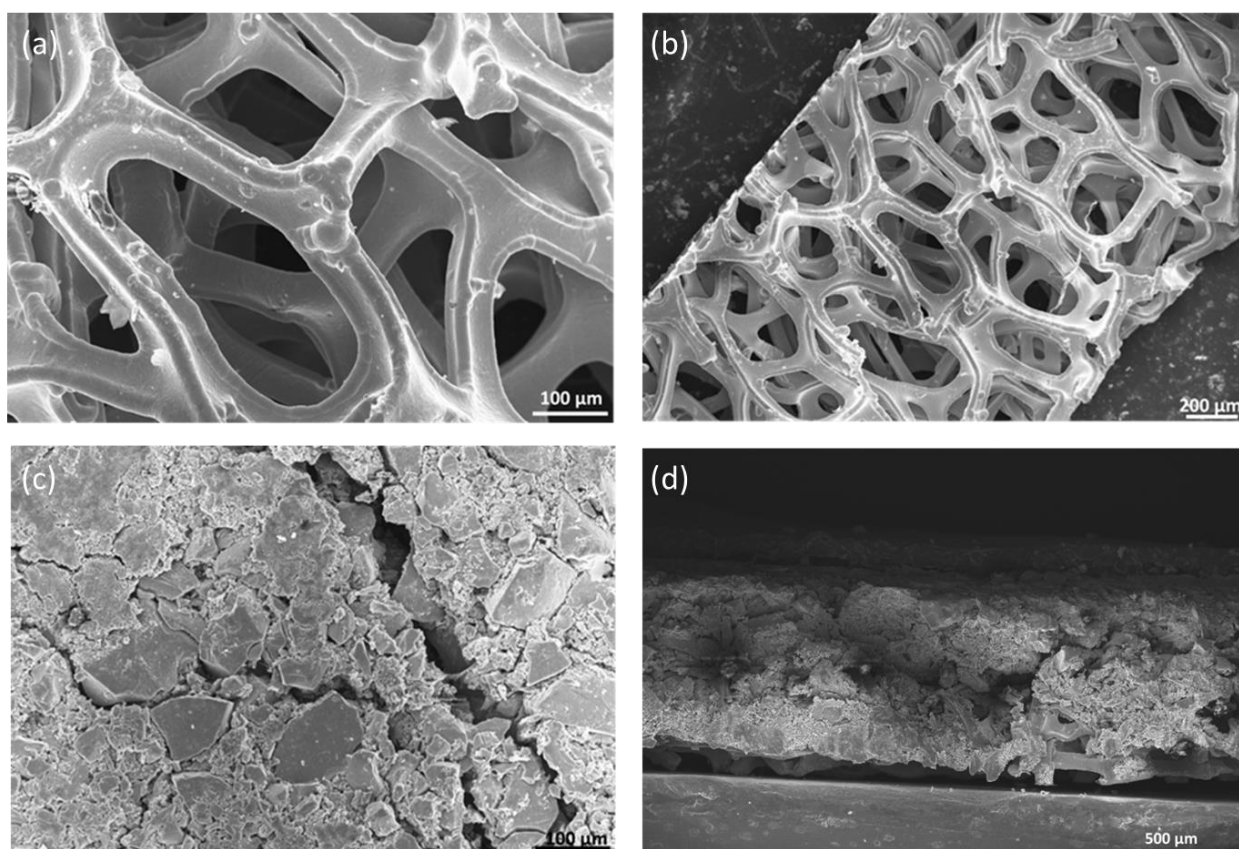


Figure 3. AEM electrolyzer configuration with AEM transporting the OH<sup>-</sup> to the anode.

### 3. Results

The morphology of the catalyst coating and nickel foams was performed by scanning electron microscope (SEM, Leo 1550, Zeiss, Jena, Germany). The morphology of nickel foam which acts as a GDL at the anode was analyzed by SEM. Figure 4a,b shows nickel foam before it was coated with the catalyst layer. The pore size was in the range of 100 to 500  $\mu\text{m}$ . Figure 4c shows nickel foam coated with  $\text{NiFeCoO}_x$  catalyst; the catalyst layer was pressed with nickel foam to get a compact layer of catalyst on top of the nickel foam. From SEM it was observed that the catalyst layer completely covered the nickel foam. There were some cracks in the catalyst layer which are due to the high loading of the catalyst. Figure 4d shows the cross-sectional image of a catalyst-coated nickel foam gas diffusion electrode (GDE), the overall thickness of GDE was 785  $\mu\text{m}$ .



**Figure 4.** SEM images of (a,b) Nickel Foam without catalyst (c)  $\text{NiFeCoO}_x$  coated on nickel foam and (d) Cross section image of nickel foam coated with  $\text{NiFeCoO}_x$  catalyst.

X-ray diffraction studies were performed (Rigaku Miniflex 600) using  $\text{Cu-K}\alpha$  radiation ( $\lambda = 1.54184 \text{ \AA}$ ). Catalysts were analyzed by XRD, commercial  $\text{NiO}$  and  $\text{NiFeO}_x$  (15% Fe) show mainly  $\text{NiO}$  phase with five distinct peaks at  $2\theta$  which are at 37.36, 43.36, 60, 75.54 and 79.56, which are assigned to (111), (200), (220), (311) and (222), respectively. All peaks are indexed to  $\text{NiO}$  (JCPDS card no. 78-0643) as shown in Figure 5. The dashed lines are the corresponding JCPDS standard.  $\text{NiO}$  has a rock salt structure with a lattice constant of 4.17  $\text{\AA}$ . Due to the low concentration of Fe in the  $\text{NiFeO}_x$  catalyst any peaks related to  $\text{NiFe}_2\text{O}_4$  or  $\text{Fe}_2\text{O}_3$  were not observed. The XRD of  $\text{NiFeCoO}_x$  catalyst which has 2.7 wt.% Fe and Ni to Co molar ratio of 2:1, showed  $\text{NiCo}_2\text{O}_4$  spinel crystal structure with a most intense peak at  $2\theta$  36.8 assigned to (311), all peaks are indexed to  $\text{NiCo}_2\text{O}_4$  (JCPDS card no. 20-0781).

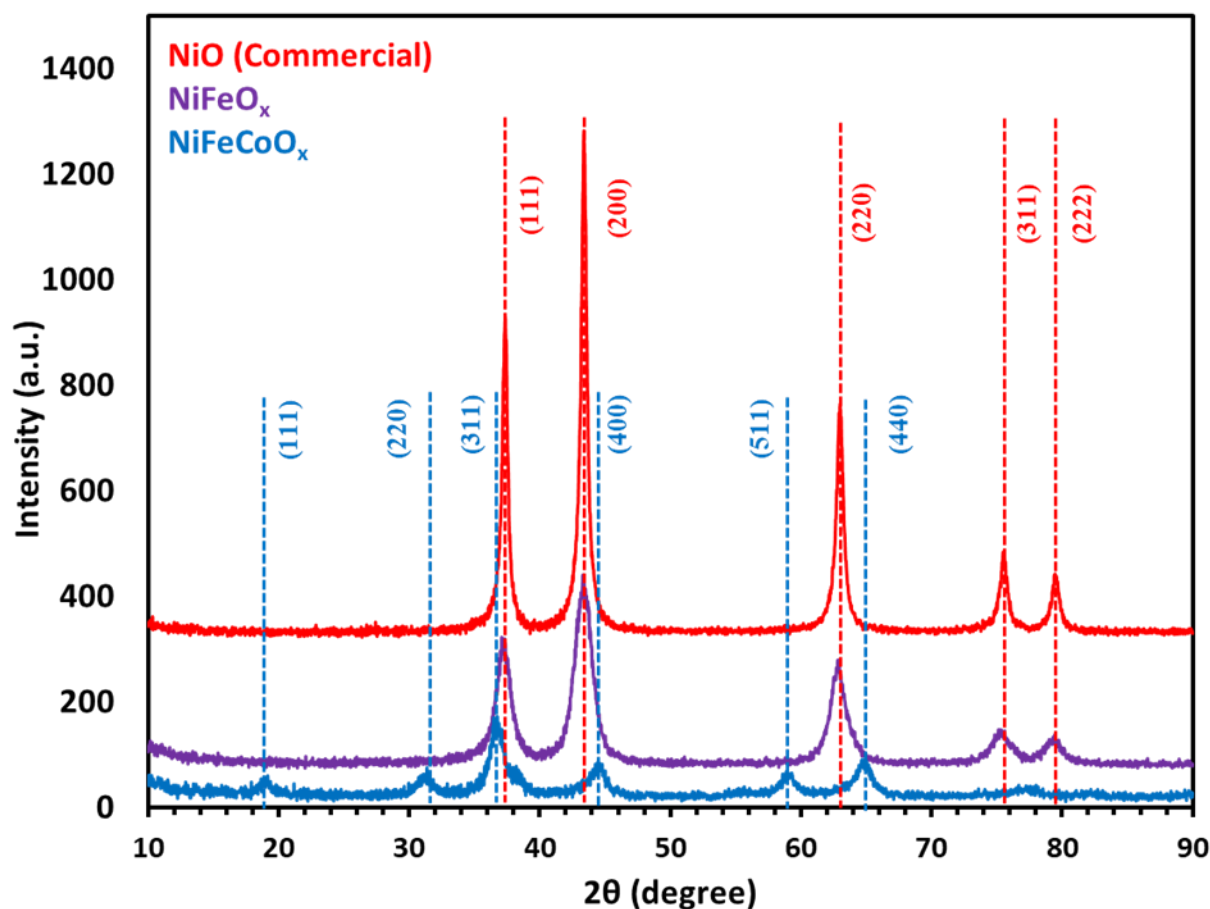


Figure 5. XRD of NiFeO<sub>x</sub>, NiFeCoO<sub>x</sub> catalyst calcined at 300 °C, commercial NiO is for reference.

Equation (4) is listed in the following, where  $\lambda$  is the wavelength of the X-ray,  $\beta$  is the full width at half Maximum (FWHM) peak intensity in radian, and  $\theta$  is the diffraction angle and  $k$  is the Scherrer's constant, which is 0.94 for crystalline nanoparticles. The calculated particle sizes for NiO, NiFeO<sub>x</sub>, and NiFeCoO<sub>x</sub> were 17, 4, and 6 nm, respectively.

$$D = \frac{k\lambda}{\beta \cos \theta} \quad (4)$$

#### 4. Water Electrolysis over NiO, NiFeO<sub>x</sub> and NiFeCoO<sub>x</sub>

Three different OER catalysts, commercial NiO, lab-made NiFeO<sub>x</sub>, and NiFeCoO<sub>x</sub> were tested for AEMWE operation with Pt/C catalyst for the HER at the cathode. The polarization curve was taken at a temperature range of 45 °C to 70 °C. LSV was used as a preferred method to evaluate the activity of the catalyst.

NiFeCoO<sub>x</sub> showed the highest activity among all the catalysts tested, the catalyst showed a current density of 802 mA cm<sup>-2</sup> at 2 V with the temperature of the electrolyte and the electrolyzer at 70 °C.

Figure 6 shows polarization curves using NiFeCoO<sub>x</sub>, at 70 °C when the voltage was further increased to 2.2 V, the current density increased to 1100 mA cm<sup>-2</sup>, which is an enhancement of about 37% in current density. The current density also increased with the increase in electrolyte temperature, for electrolysis operation at 45 °C and 55 °C at 2 V. The current density was 532 and 656 mA cm<sup>-2</sup>, which increased to 802 mA cm<sup>-2</sup> at 70 °C, which is an increase of 53% and 22% in the current density. The increase in temperature decreases the overpotential at the cathode and anode side for OER and hydrogen evolution reaction (HER). Moreover, the conductivity of the electrolyte also increased with the temperature and improves the overall activity of the electrolysis [4]. In another study, electrolysis

performance was evaluated from 30 °C to 50 °C, at the current density of 470 mA cm<sup>-2</sup>. The electrolyzer potential decreased with the increase in temperature [29]. The effect of temperature was also investigated with a novel integrated inorganic membrane electrode assembly at the temperature range of 50–70 °C, the performance of the electrolyzer improves with the increase in temperature. The enhancement in the performance was mainly due to the higher conductivity of OH<sup>-</sup> and the reduction in the overpotential of the catalyst [32]. It has been reported that the addition of cobalt in NiO lattice results in the formation of conductive Ni<sup>III</sup>OOH. Fe content in the range of 10–20% has been shown to improve the NiO catalyst performance for OER. Fe was proposed to stabilize Ni in the Ni<sup>2+</sup> Oxidation state and Co helps in the formation of Ni<sup>3+</sup> [33].

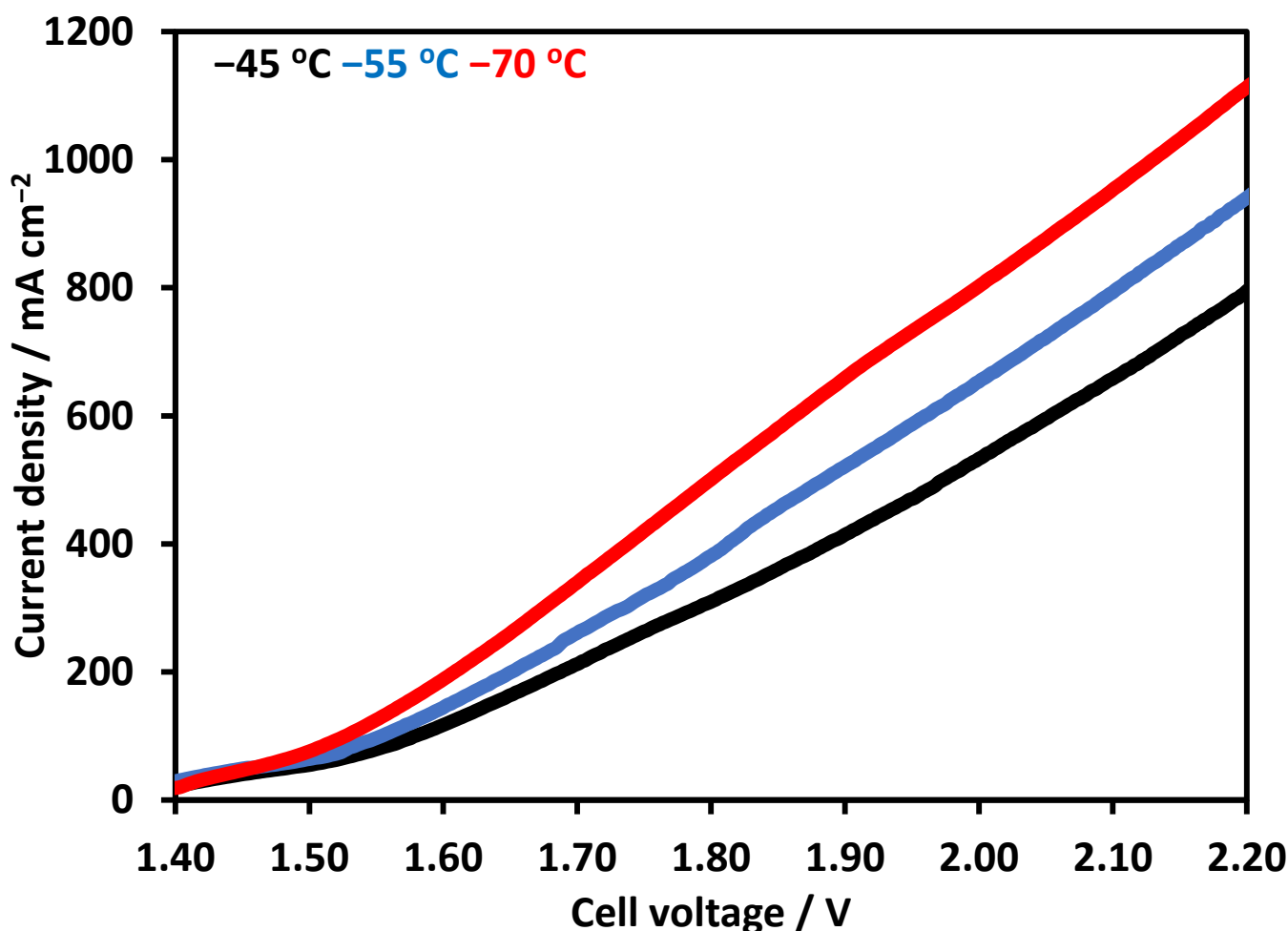


**Figure 6.** Linear Sweep Voltammetry at temperature range of 45 to 70 °C. Pt/C was used at cathode and synthesized NiFeCoO<sub>x</sub> was used at anode. FAA-3-50 membrane with a thickness of 50 μm was used in electrolysis operation.

Chronoamperometry was used to analyze the activity of the catalyst at constant voltage for a fixed period of time. Figure 7 shows the chronoamperometry at 70 °C. The voltage increased from 1.5 V to 2.2 V with a time step of 60 s. The electrolysis operation was stable during the analysis and had minimum current fluctuations at the fixed voltage. At 2.2 V the maximum current density was 1140 mA cm<sup>-2</sup>.

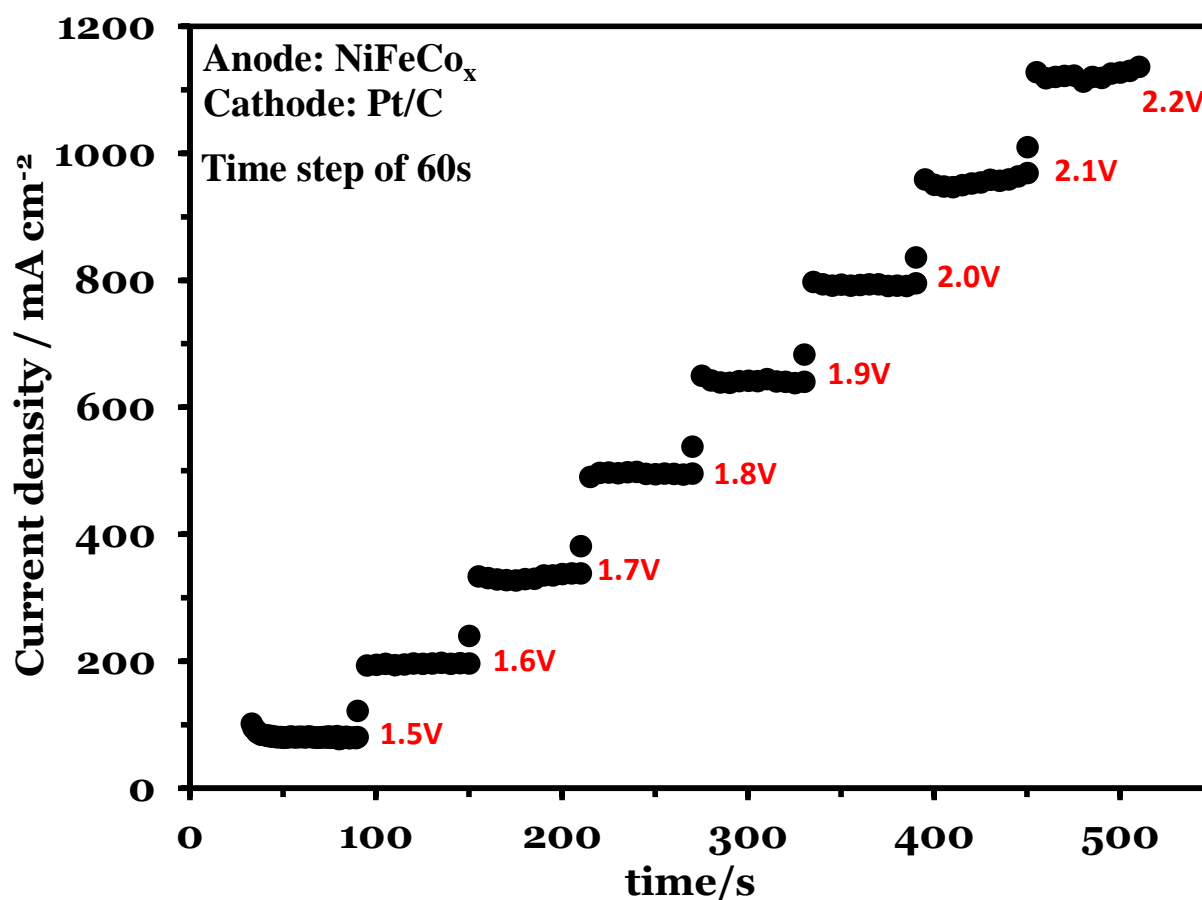
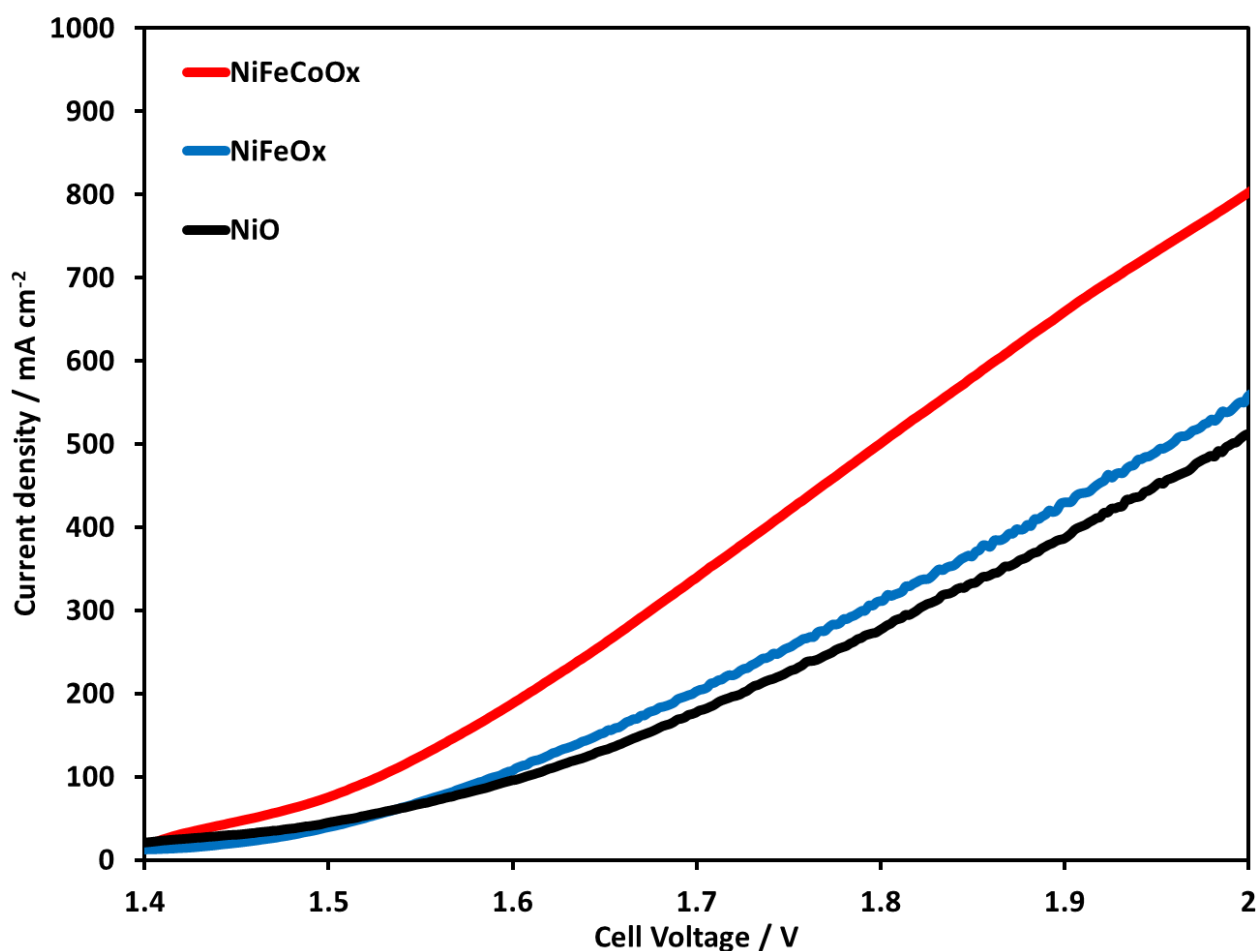


Figure 7. Chronoamperometry at a voltage range of 1.5 to 2.2 V, Pt/C was used at the cathode and NiFeCoO<sub>x</sub> was used at anode.

Figure 8 shows the LSV of NiO, NiFeO<sub>x</sub>, and NiFeCoO<sub>x</sub> catalysts at 70 °C using 1 M KOH electrolyte. NiFeCoO<sub>x</sub> had a higher current density followed by NiFeO<sub>x</sub> and NiO, the current density with NiFeO<sub>x</sub> catalyst was 551 and with NiO was 509 mA cm<sup>-2</sup>. When comparing the performance of NiO and NiFeO<sub>x</sub>, there was not much enhancement due to the addition of Fe in the NiFeO<sub>x</sub> catalyst. In this study, very high loading of Fe was used which might have decreased the performance of the NiFeO<sub>x</sub> catalyst. Ni-Fe-based catalysts are reported to have higher catalytic activity in basic electrolyte medium [34,35]. Nickel is proposed to be an active site for OER and Fe is considered to improve the conductivity of the catalyst. In other research works, the addition of Fe is linked to stabilize Ni in Ni<sup>2+</sup> form [36]. Ni-Fe binary catalyst modified with third metal (Cr, Mo, and V) showed higher activity compared to the Ni-Fe oxide catalyst [37–39].

Emily Cossar et al. studied the AEMWE performance over Ni-Fe nanoparticles as anodes using 1 M KOH, Ni<sub>0.9</sub>Fe<sub>0.1</sub> showed the cell voltage of 1.72 V at 0.8 A.cm<sup>-2</sup>. Ni<sub>0.80</sub>Fe<sub>0.1</sub> with 10% CeO<sub>2</sub> had a voltage of 1.67 V with 0.4 A.cm<sup>-2</sup> using 0.1 M KOH. In durability testing, Ni<sub>0.9</sub>Fe<sub>0.1</sub> showed stability of 12 h at 0.5 A.cm<sup>-2</sup> [40]. In another study, NiFe bimetallic anodes were fabricated using the magnetron sputtering technique. The work showed the enhancement in electrochemical activity with the addition of Fe to Ni-based catalysts. The highest performance was on Ni/Fe catalyst with an atomic ratio of 10/1, on that catalyst at 2 V the current density was 0.6 A.cm<sup>-2</sup> and 0.4 A.cm<sup>-2</sup> at 60 °C and 40 °C, respectively [41]. Dongyu Xu et al. synthesized transition metal (oxy) hydroxide for OER and tested it in the AEM electrolyzer. Among the catalysts NiCoO<sub>x</sub>:Fe showed the highest activity with a current density of 900 mA cm<sup>-2</sup> at 2.4 V [42]. The catalyst was designed to be oxyhydroxide because the active sites for OER are proposed to be transition metal oxyhydroxide.



**Figure 8.** Linear Sweep Voltammetry at temperature of 70 °C. Pt/C was used at the cathode and NiO, NiFeO<sub>x</sub>, and NiFeCoO<sub>x</sub> were used at anode. FAA-3-50 membrane with a thickness of 50 μm was used in electrolysis operation.

EIS measurements were carried out to get the impedance of the electrolyzer cell during the operation. Potentiostatic EIS was performed at the voltage range of 1.7 V to 2 V, with a frequency range of 100 kHz to 100 mHz, the data was analyzed by Nyquist plots and equivalent circuit fitting. Figure 9 shows the Nyquist plot for electrolysis operation performed at 1.7 V at two different temperatures of 45 °C and 70 °C. The first x-intercept is at a high-frequency region and shows the ohmic resistance ( $R_{ohm}$ ), the second intercept at the x-axis subtracted by the first intercept gives the activation resistance ( $R_{act}$ ). As can be seen in Figure 9, the diameter of the semicircle for the Nyquist plot at 45 °C is higher which shows that there is higher activation resistance at this temperature compared to 70 °C operation. To further evaluate the contribution of different components to the resistance, the equivalent circuit fitting is performed. The circuit given in Figure 9 shows the whole electrolyzer element, where L is the inductance due to the wires, R1 is the ionic resistance due to the AEM, R2, and R3 are the activation resistance due to the anode and cathode, respectively. Q1 and Q2 at anode and cathode are the constant phase element (CPE) and are used to simulate resistors, capacitors, and inductors, and capture the effects of surface roughness, porosity, reactivity, and surface inhomogeneity that are due to the electrical double layer [43]. EC-Lab software was used to fit the Nyquist plot with Randomize simplex method and the results are given in Table 1.

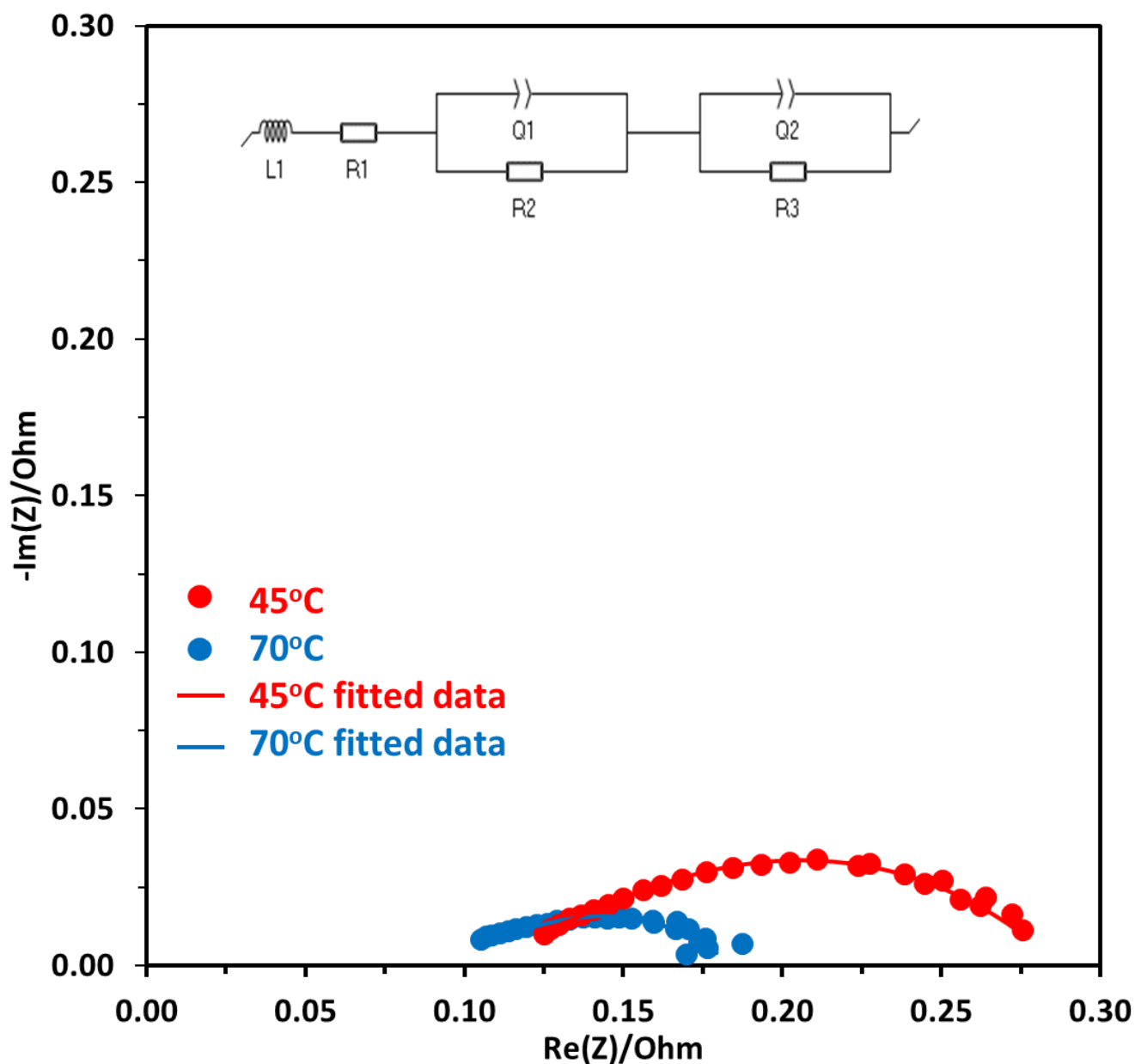


**Figure 9.** Nyquist plot at a constant voltage of 1.7 V at two different temperatures of 45 °C and 70 °C, Pt/C was used at the cathode and NiFeCoO<sub>x</sub> was used at the anode.

**Table 1.** Resistances evaluated from equivalent circuit fitting.

Resistance	Temperature	
	45 °C	70 °C
R <sub>ohm</sub>	0.125	0.105
R <sub>membrane</sub>	0.102	0.068
R <sub>anode</sub> + R <sub>cathode</sub>	0.186	0.116

Equivalent circuit results are tabulated in Table 1. As the electrolyzer was operated at a higher temperature of 70 °C, the ohmic resistance decreased from 0.125 to 0.105 Ω. This was mainly due to the increase in the conductivity of OH<sup>-</sup> at higher temperatures, which also results in a decrease in membrane resistance. The ohmic losses are due to the resistance in the flow of electrons from different components of the electrolyzer, such as the anode, cathode, and membrane.

The total activation resistance at the anode and cathode were also evaluated using equivalent circuit fitting. With the increase in temperature, the total activation resistance at both electrodes decreased from 0.186 to 0.116  $\Omega$ . This is mainly due to the improvement of reaction kinetics of OER and improved conductivity of  $\text{OH}^-$  with the increase in temperature. The membrane resistance also decreased with the increase in temperature and there was a reduction of about 33%, when the temperature was increased from 45 to 70  $^\circ\text{C}$ . One of the reasons for the decrease in ohmic resistance is the decrease in the membrane resistance with the temperature. It was reported that the membrane resistance decreased from 75.3 to 52.5  $\text{m}\Omega\cdot\text{cm}^2$  for polycarbazole-based anion exchange membrane (QPC-TM) [10].

The EIS measurement at a voltage of 1.9 V was performed by Immanuel Vincent et al., the ohmic resistance was reported to decrease with the increase in temperature. The reported ohmic resistance at 1.9 V was 17.8, 16, 15.8, and 15.6  $\text{m}\Omega$  at 30, 40, 50, and 60  $^\circ\text{C}$  [44]. In PEM electrolysis, an increase in temperature is also reported to decrease the ohmic contact, one of the reasons being the thermal expansion of the components which causes the decrease in interfacial contact resistance [45,46]. The interfacial contact resistance decreases with the thermal expansion due to the increased compression pressure in the PEM electrolyzer [47].

## 5. Effect of Electrolyte Concentration

The concentration of the electrolyte is an important parameter that needs to be understood in detail to optimize the electrolysis conditions. It is desirable to operate the electrolyzer at low electrolyte concentrations or only with water. However, using only water or using low concentrations of the electrolyte can significantly affect the performance of the electrolyzer, due to the decreased conductivity of  $\text{OH}^-$  ions.

In this work, the electrolyzer was tested at three different concentrations of KOH. The molarity of KOH was 0.01, 0.1, and 1 M used in this study, all other parameters were the same as mentioned earlier. Briefly, 25  $\text{mg}/\text{cm}^2$  NiFeCoO<sub>x</sub> catalyst at the anode side and 1  $\text{mg}_{\text{Pt}}/\text{cm}^2$  Pt/C were used at the cathode, the anion membrane was 50  $\mu\text{m}$  Faumsep FAA-3-50. Figure 10 shows the LSV curves, the highest activity was achieved when 1 M KOH was used, and the electrolyzer reached the current density of 951, 681, and 513  $\text{mA cm}^{-2}$  for 1 M, 0.1 M and 0.01 M electrolyte at 2.1 V. The current density increased to about 39%, when electrolyte concentration increased from 0.01 M to 0.1 M, and there was an increase of 85% in current density when KOH concentration increased from 0.01 to 1 M. It was also observed that at 0.01 M concentration, the polarization curve did not remain linear after 1.9 V and slightly bend downwards. This is the indication that at a higher voltage, more  $\text{OH}^-$  is required for the OER, but due to the lower concentration of  $\text{OH}^-$ , the current density did not remain linear and started to decrease. This trend was not observed for 0.1 M and 1 M concentration electrolyzer performance. Electrolysis with DI water has shown lower current density compared with other results obtained with KOH, the highest current density achieved was 254  $\text{mA cm}^{-2}$  at 2.1 V. At 2.3 V, which is considered high for electrolysis, the current density was 400  $\text{mA cm}^{-2}$ .

An increase in pH is reported to improve the conductivity of AEM, which reduces the ohmic resistance and increases the activity of AEMWE operations [48]. Higher pH is reported to decrease the overpotential of the reaction. At lower concentrations of KOH there is a lower number of  $\text{OH}^-$  available, which causes slower reaction kinetics of OER [4]. In other works, DI water was used in AEM electrolyzer with a current density of 399  $\text{mA cm}^{-2}$  at 1.8 V [30]. At a current density of 400  $\text{mA cm}^{-2}$  with ultra-pure water, an electrolyzer voltage of 1.8 V is reported [31].

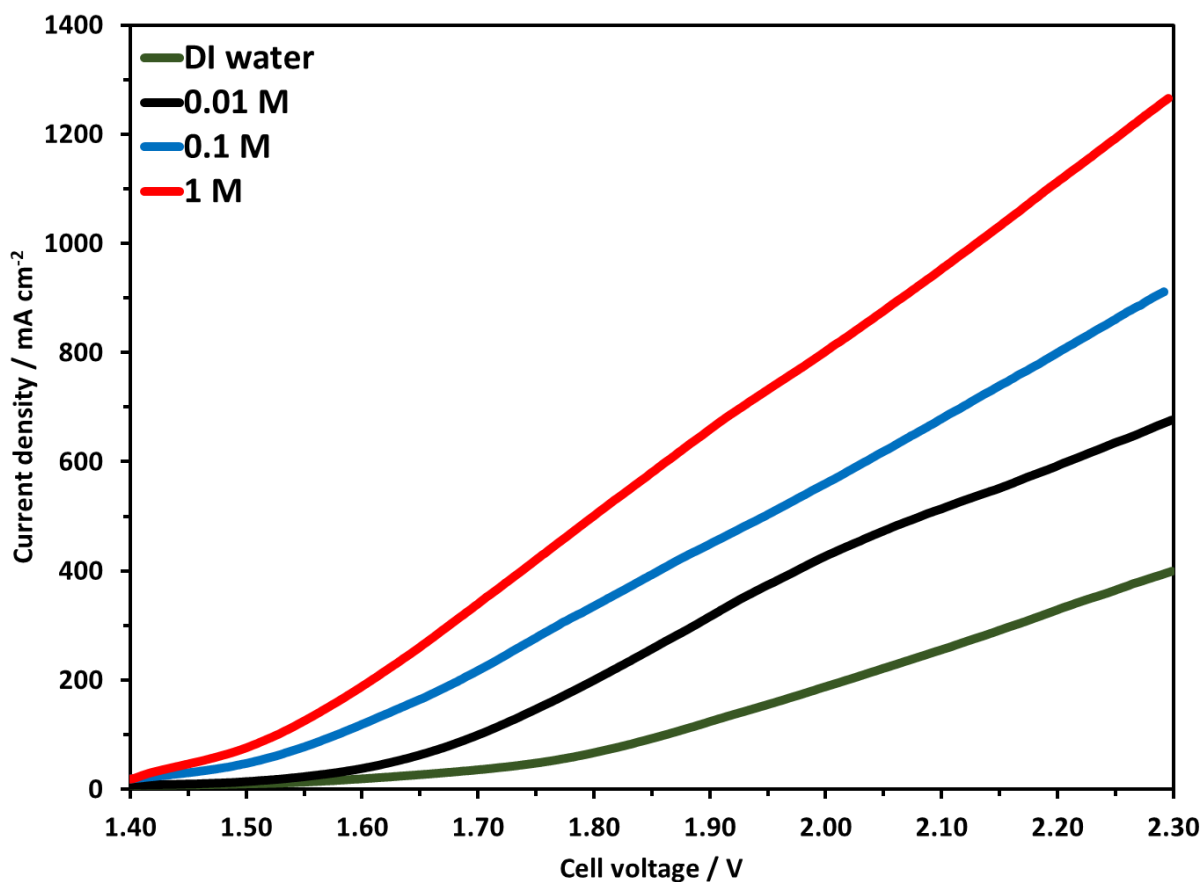


**Figure 10.** Linear Sweep Voltammetry at temperature of 70 °C with 0.01 M to 1 M KOH concentration. Pt/C was used at the cathode and NiFeCoO<sub>x</sub> was used at anode.

Nyquist plot for KOH concentration of 0.01 M to 1 M and DI water are shown in Figure 11a,b. The EIS was performed at 2 V and 70 °C for all electrolyte concentrations. There is a big difference between the DI water Nyquist plot, which has a higher x-intercept and a bigger diameter, which are indicative of ohmic resistance and activation resistance, respectively. The ohmic resistance for DI water-fed electrolyzer was very high at 0.56 Ω. For KOH-fed electrolyzer the ohmic resistance decreased with the increase in concentration. Lower ohmic resistance with increased KOH concentration was due to the increased conductivity of the anion exchange membrane.

For comparison, the ohmic resistance using 1 M KOH was 0.12 Ω, which was 4.66 times lower compared to the DI water-fed electrolyzer. For EIS measurement at 1.5 V, ohmic resistance is reported to decrease from 170.4 to 18 mΩ, when the concentration of KOH increased from 0 to 1 M KOH [44]. The decrease in ohmic resistance was attributed to the increase in the conductivity of the membrane.

To evaluate individual resistances due to the components of the electrolyzer, equivalent circuit fitting was performed with the same circuit as discussed earlier. The results from the equivalent circuit fitting are shown in a bar graph in Figure 12. The Figure shows the activation resistance at the anode and cathode along with membrane resistance, the resistances as a function of electrolyte are shown along with DI water. In all cases, DI water shows the highest resistances at each component of the electrolyzer, followed by 0.01 M and 0.1 M KOH. These results showed that two main components which can control the activity of the electrolyzer are the anion exchange membrane and the anode catalyst. For the membrane, a lower thickness and higher conductivity can reduce these resistances. For the resistance at the anode, where an oxygen evolution reaction takes place, there is still room for improving the OER catalyst to reduce the overpotential of the catalyst. Another trend that was observed was membrane resistance and activation resistance at the anode

decreased with the increase in KOH concentration, but activation resistance at the cathode did not change much with the increase in KOH concentration.

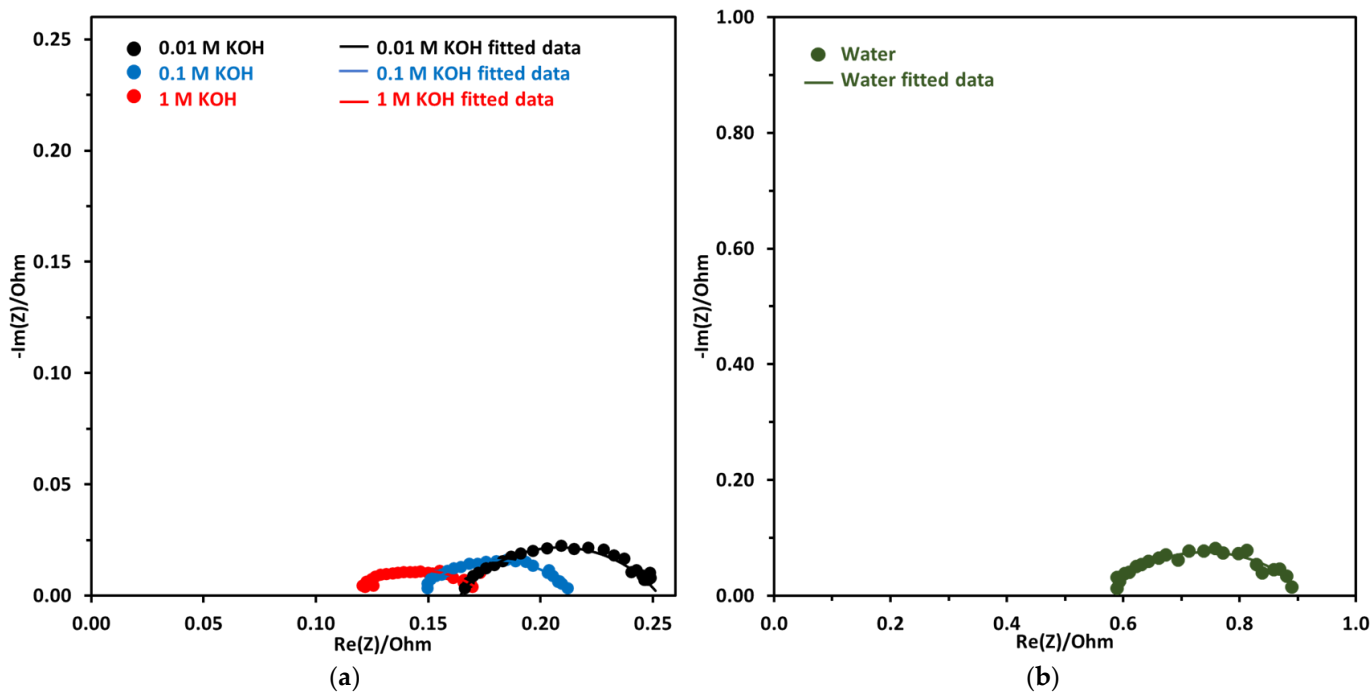


**Figure 11.** (a) Nyquist plot at a constant voltage of 2 V at 70 °C, the concentration of electrolyte was from 0.01 M to 1 M. (b) Nyquist plot using DI water. Pt/C was used at the cathode and NiFeCoO<sub>x</sub> was used at anode with FAA-3-50 membrane.

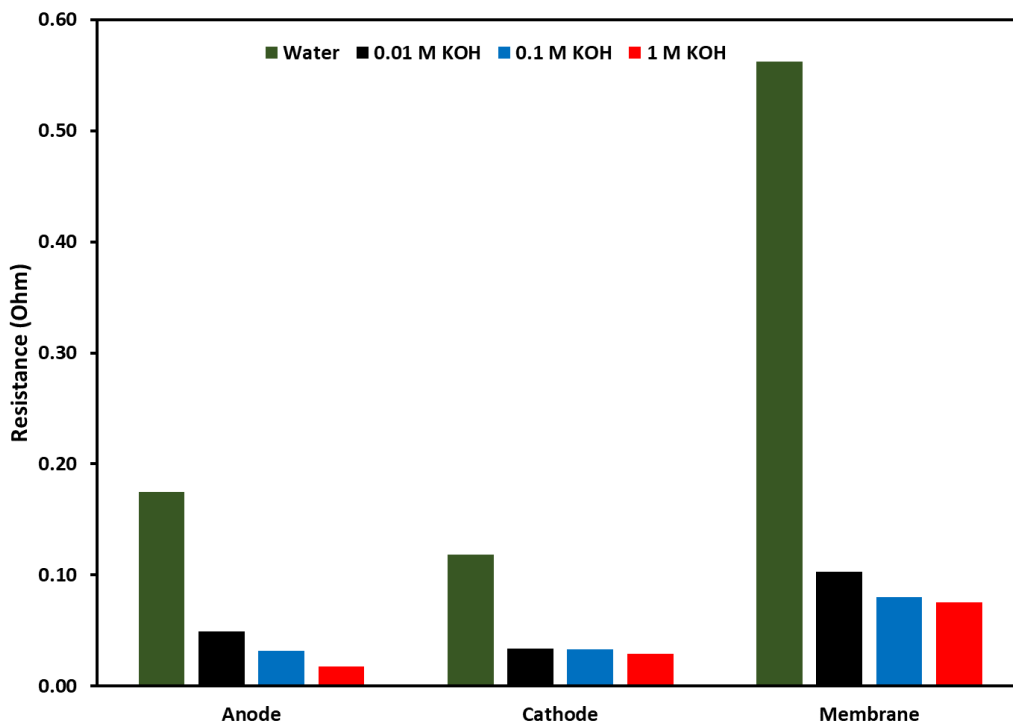


**Figure 12.** Comparison of resistances at anode, cathode, and membrane, the resistances were evaluated by using equivalent circuit fitting. The applied voltage was 2 V at 70 °C.

## 6. Comparison of AEM Membranes

The AEM is the main component of the electrolysis cell. It is made up of a polymer backbone and functionalized with anion exchange groups, mostly with quaternary ammonium salts [49,50]. AEM membrane should have the properties of high ionic conductivity, good thermal and mechanical stability, gas impermeability and stability in long-term usage [51–53]. Its main role is to transport  $\text{OH}^-$  from the cathode to the anode side, and to avoid gas crossover. To be considered for commercial use, AEM should be of low cost to increase its feasibility. Membrane conductivity is shown to increase with the nucleophilic substitution of the ammonium group and by the substitution of a methyl group to hydroxyl ions. High conductivity can be achieved with the increase in the incorporation of the anion exchange group, but it may also increase the water uptake and deteriorate the mechanical strength of the membrane [11].

Commercially available AEM membranes are widely used in AEM electrolysis research, which are Sustainion<sup>®</sup> 37-50 (dioxide membrane), Tokuyama A201, Fumasep<sup>®</sup> FAA-3, Orion<sup>™</sup>, and Aemion<sup>™</sup>. These AEM needs to be pretreated because they are usually shipped in bromide and chloride forms. The AEM can be activated by keeping the membrane in the KOH solution for about 24 to 48 h. Table 2 provides the properties of the commercially available membrane [42,54–56].

**Table 2.** Commercially available membranes and their properties [52,57,58].

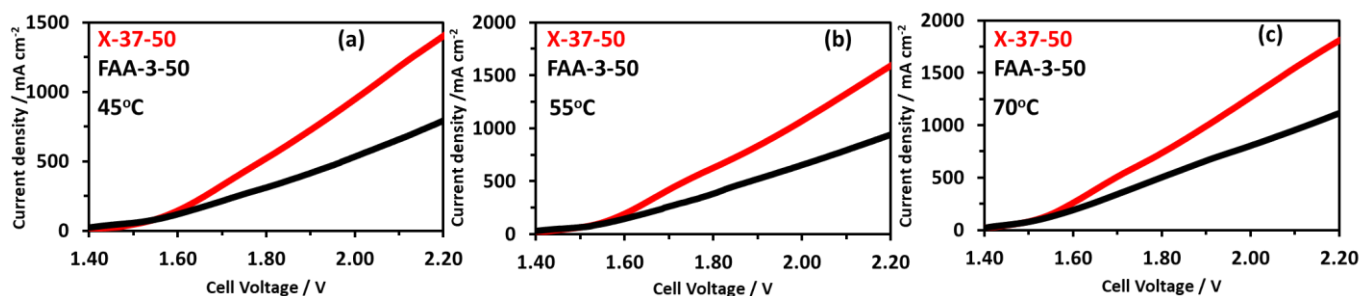
Membrane	Thickness ( $\mu\text{m}$ )	Conductivity ( $\text{ms}\cdot\text{cm}^{-1}$ )
Sustainion <sup>®</sup> 37–50 (dioxide membrane)	50	70
Fumasep <sup>®</sup> FAA-3	45–50	40–45
Fumasep <sup>®</sup> FAB-PK-130	110–140	42
Tokuyama A201	28	-
Aemion <sup>™</sup>	50	80
Orion <sup>™</sup>	50	60

Membranes from Fumatech, such as the FAA3 type, are polyaromatic polymers with ether bonds and quaternary ammonium group present at the main chain. The reported electrolysis work with these membranes in the presence of a noble metal catalyst (Pt/C cathode and  $\text{IrO}_2$  anode) showed the activity of  $1.5 \text{ A}\cdot\text{cm}^{-2}$  at 2 V with 1 M KOH at  $50^\circ\text{C}$  [59]. The durability testing of the FAA3-40 membrane showed a lifetime of 31 h, due to poor mechanical stability caused by the excessive swelling of the membrane [4]. Whereas, the FAA3-50 AEM membrane shows the stability of 1000 h, with the  $\text{NiMnO}_x$  anode and Pt/C cathode catalyst [60]. Sustainion membranes X-37-50 from dioxide materials are based on 4-vinylbenzyl chloride-co-styrene [51,52,61]. The membranes take some water for crosslinking which reduces the swelling of the membrane during the electrolysis operation [52].

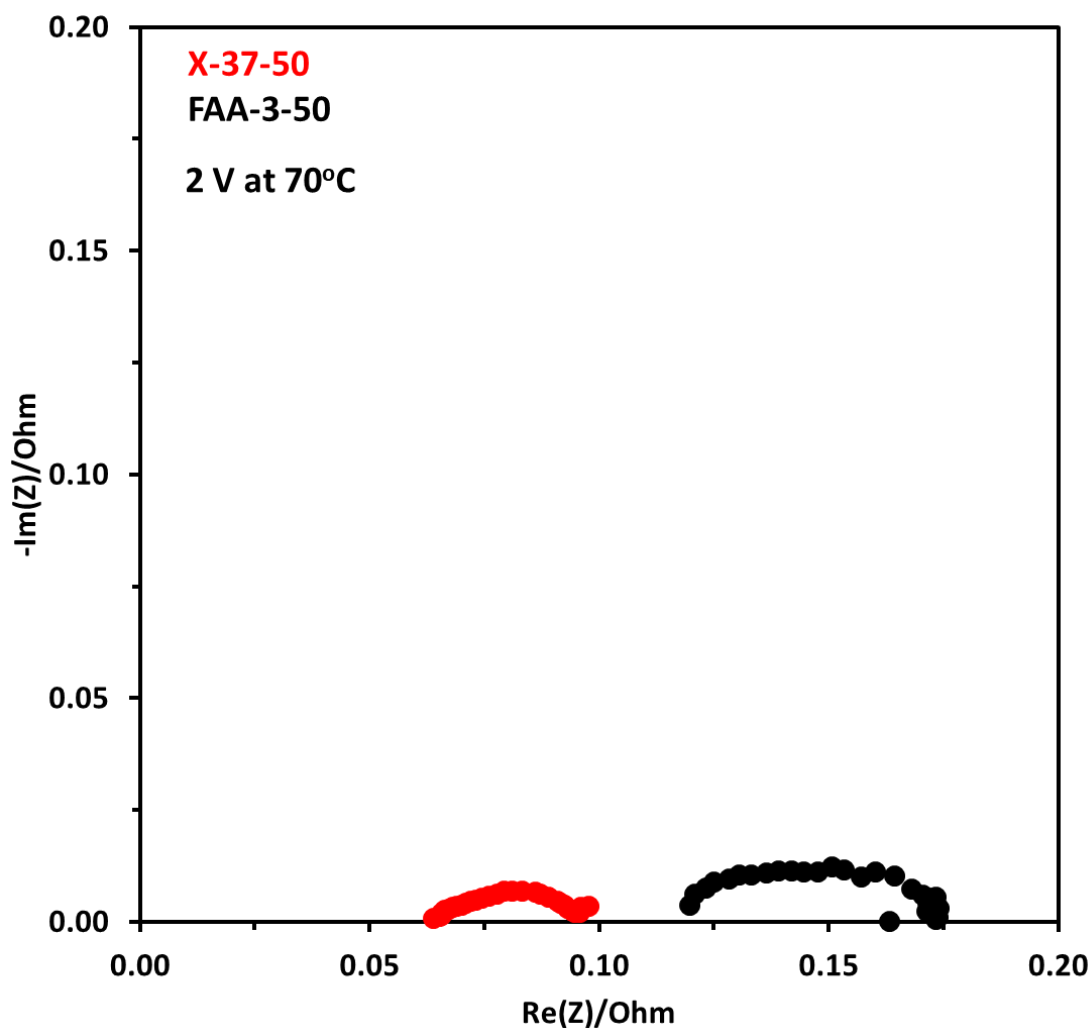
For the comparison of electrolyzer activity commercially available Dioxide membrane X-37-50 was used, the MEA preparation method was similar as mentioned earlier. The operation was performed at three temperatures of 45, 55, and  $70^\circ\text{C}$  as shown in Figure 13a–c. The X-37-50 MEA had a higher current density at each temperature compared to the FAA-3-50 membrane with the same thickness of  $50 \mu\text{m}$ . At 2.2 V the current density for X-37-50 MEA was 1390, 1590, and 1815, for FAA-3-50 MEA it was 794, 937, and  $1121 \text{ mA cm}^{-2}$  at 45, 55, and  $70^\circ\text{C}$ , respectively. The higher activity could be correlated with the X-37-50 higher conductivity compared to the FAA-3-50 membrane. With a non-precious catalyst, Sustainion 37–50 membrane showed stability for 2000 h while maintaining the current density of  $1 \text{ A}\cdot\text{cm}^{-2}$  at 1.9 V [51,52]. With Platinum and  $\text{IrO}_2$  catalysts at the cathode and anode, respectively,  $2 \text{ A}\cdot\text{cm}^{-2}$  of current density was reported at a very low voltage of 1.7 V [52,62].

Figure 14 shows EIS results at  $70^\circ\text{C}$  for both membrane electrode assemblies at 2 V. There is a big difference between both results. The ohmic resistance for the X-37-50 was  $0.064 \Omega$  and for FAA-3-50 it was  $0.12 \Omega$ . This shows that the conductivity of the X-37-50 is higher in similar conditions, higher conductivity decreases the resistance caused by the

membrane. This also demonstrated that the X-37-50 membrane has better charge transfer ability between the catalyst layer and the membrane compared to FAA-3-50. The diameter of the semicircle which is indicative of activation resistance is also lower for X-37-50, the corresponding activation resistance was 0.037 and 0.054  $\Omega$ . These results showed that lower ohmic resistance and activation resistance resulted in higher performance for X-37-50.



**Figure 13.** Comparison of electrolysis performance using X-37-50 and FAA-3-50 membranes at different temperatures using  $\text{NiFeCoO}_x$  catalyst; (a) 45 °C, (b) 55 °C, (c) 70 °C.



**Figure 14.** Nyquist plot at constant voltage of 2 V at 70 °C with FAA-3-50 and X-37-50 anion exchange membranes, the concentration of electrolyte was 1 M. Pt/C was used at the cathode and  $\text{NiFeCoO}_x$  was used at anode.

There are few studies where Sustainion X-37-50 is reported to be a better membrane in terms of stability and performance. Electrochemical impedance comparison at different membranes showed Sustainion<sup>®</sup> 37-50 had lower resistance compared to Fumasep<sup>®</sup> FAS-50, Fumasep<sup>®</sup> FAPW, AMI 7001, and Nafion 115. When it was compared with Aemion<sup>™</sup> and Tokuyama A201 membranes at different temperatures, electrolyte, and current density, the Sustainion membrane showed higher performance with 3 A cm<sup>-2</sup> current density with 1 M KOH at 60 °C [63]. Sustainion<sup>®</sup> membrane had higher stability in the test with a degradation rate of 5 μV.h<sup>-1</sup> for 2000 h operation at a fixed current density of 1 A.cm<sup>-2</sup> [50]. Tokuyama A201 had a degradation rate of 150 μV.h<sup>-1</sup> for 1000 h at 470 mA cm<sup>-2</sup> [29], Fumasep<sup>®</sup> FAA-3-50 had a degradation rate of 800 μV h<sup>-1</sup> in 1000 h [60].

## 7. Conclusions

NiO, NiFeO<sub>x</sub>, and NiFeCoO<sub>x</sub> catalysts were tested for AEMWE using Fumasep FAA-3-50 membrane, NiFeCoO<sub>x</sub> showed higher performance than other catalysts, due to the promotion effect of Co and Fe in Ni-based catalysts. The highest activity at 2 V with NiFeCoO<sub>x</sub> catalysts was 802 mA cm<sup>-2</sup> at 70 °C. The performance of the AEM electrolyzer was found to be highly dependent on the electrolyte concentration, the activity was 954 mA cm<sup>-2</sup> at 2.1 V with 1 M KOH whereas with DI water it was 254 mA cm<sup>-2</sup> at 70 °C. EIS results showed that there is a decrease in ohmic resistance with the increase in electrolyte concentration, mainly due to the increased conductivity of the membrane. The membrane conductivity increased due to more OH<sup>-</sup> ions available at higher concentrations of KOH. The activation resistance of the anode also decreased with the increase in electrolyte concentrations, which is due to the availability of more OH<sup>-</sup> ions at higher pH, which improved the reaction kinetics of OER. A comparison of the FAA-3-50 and X-37-50 membranes, which have the same thickness of 50 μm showed higher AEM electrolyzer performance with the X-37-50 membrane. For comparison, the highest activity on FAA-3-50 and X-37-50 membrane was 1121 and 1815 mA cm<sup>-2</sup> at 2.2 V, 70 °C, which shows X-37-50 had 1.62 times higher current density at the same operating conditions. EIS results showed that the X-37-50 membrane had lower ohmic resistance than the FAA-3-50 membrane.

**Author Contributions:** K.W.A.: Conceptualization, Methodology, Data curation, Writing—original draft, Visualization. M.J.J.: Reviewing and modifying the original draft. S.H. performing SEM analysis, Z.C.: Review and editing, Supervision, Project administration, Funding acquisition. M.F.: Conceptualization, Methodology, Supervision, Project administration, Funding acquisition. All authors have read and agreed to the published version of the manuscript.

**Funding:** This research received no external funding.

**Institutional Review Board Statement:** Not applicable.

**Informed Consent Statement:** Not applicable.

**Data Availability Statement:** Open source.

**Acknowledgments:** This work was supported by the Department of Chemical Engineering at the University of Waterloo, Canada Research Chair Tier I—Zero-Emission Vehicles and Hydrogen Energy Systems Grant number: 950-232215. The authors acknowledge the support from the University of Waterloo and Waterloo Institute for Nanotechnology, Natural Sciences and Engineering Research Council of Canada (NSERC).

**Conflicts of Interest:** The authors declare that they have no known competing financial interests or personal relationships that could have appeared to influence the work reported in this paper.

## References

1. Yang, J.; Jang, M.J.; Zeng, X.; Park, Y.S.; Lee, J.; Choi, S.M.; Yin, Y. Non-precious electrocatalysts for oxygen evolution reaction in anion exchange membrane water electrolysis: A mini review. *Electrochem. Commun.* **2021**, *131*, 107118. [[CrossRef](#)]
2. Motealleh, B.; Liu, Z.; Masel, R.I.; Sculley, J.P.; Ni, Z.R.; Meroueh, L. Next-generation anion exchange membrane water electrolyzers operating for commercially relevant lifetimes. *Int. J. Hydrog. Energy* **2021**, *46*, 3379–3386. [[CrossRef](#)]

3. Faid, A.Y.; Barnett, A.O.; Seland, F.; Sunde, S. NiCu mixed metal oxide catalyst for alkaline hydrogen evolution in anion exchange membrane water electrolysis. *Electrochim. Acta* **2021**, *371*, 137837. [[CrossRef](#)]
4. Vincent, I.; Kruger, A.; Bessarabov, D. Development of efficient membrane electrode assembly for low cost hydrogen production by anion exchange membrane electrolysis. *Int. J. Hydrog. Energy* **2017**, *42*, 10752–10761. [[CrossRef](#)]
5. Marini, S.; Salvi, P.; Nelli, P.; Pesenti, R.; Villa, M.; Berrettoni, M.; Zangari, G.; Kiros, Y. Advanced alkaline water electrolysis. *Electrochim. Acta* **2012**, *82*, 384–391. [[CrossRef](#)]
6. Ahmed, K.W.; Jang, M.J.; Park, M.G.; Chen, Z.; Fowler, M. Effect of Components and Operating Conditions on the Performance of PEM Electrolyzers: A Review. *Electrochem* **2022**, *3*, 581–612. [[CrossRef](#)]
7. Wu, X.; Scott, K.  $\text{Cu}_x\text{Co}_{3-x}\text{O}_4$  ( $0 \leq x < 1$ ) nanoparticles for oxygen evolution in high performance alkaline exchange membrane water electrolyzers. *J. Mater. Chem.* **2011**, *21*, 12344–12351.
8. Jang, M.J.; Yang, J.; Jeong, J.; Kim, G.H.; Kwon, C.Y.; Myung, N.V.; Lee, K.H.; Choi, S.M. Promotion Effect of Modified Ni/C by La–Ce Oxide for Durable Hydrogen Evolution Reaction. *ACS Sustain. Chem. Eng.* **2021**, *9*, 12508–12513. [[CrossRef](#)]
9. Jang, M.J.; Yang, J.; Lee, J.; Park, Y.S.; Jeong, J.; Park, S.M.; Jeong, J.; Yin, Y.; Seo, M.; Choi, S.M. Superior performance and stability of anion exchange membrane water electrolysis: pH-controlled copper cobalt oxide nanoparticles for the oxygen evolution reaction. *J. Mater. Chem. A* **2020**, *8*, 4290–4299. [[CrossRef](#)]
10. Jang, M.J.; Yang, S.H.; Park, M.G.; Jeong, J.; Cha, M.S.; Shin, S.; Lee, K.H.; Bai, Z.; Chen, Z.; Lee, J.Y. Efficient and Durable Anion Exchange Membrane Water Electrolysis for a Commercially Available Electrolyzer Stack using Alkaline Electrolyte. *ACS Energy Lett.* **2022**, *7*, 2576–2583. [[CrossRef](#)]
11. Vincent, I.; Bessarabov, D. Low cost hydrogen production by anion exchange membrane electrolysis: A review. *Renew. Sustain. Energy Rev.* **2018**, *81*, 1690–1704. [[CrossRef](#)]
12. Bockris, J.O. Kinetics of activation controlled consecutive electrochemical reactions: Anodic evolution of oxygen. *J. Chem. Phys.* **1956**, *24*, 817–827. [[CrossRef](#)]
13. Song, F.; Bai, L.; Moysiadou, A.; Lee, S.; Hu, C.; Liardet, L.; Hu, X. Transition metal oxides as electrocatalysts for the oxygen evolution reaction in alkaline solutions: An application-inspired renaissance. *J. Am. Chem. Soc.* **2018**, *140*, 7748–7759. [[CrossRef](#)] [[PubMed](#)]
14. Lu, F.; Zhou, M.; Zhou, Y.; Zeng, X. First-row transition metal based catalysts for the oxygen evolution reaction under alkaline conditions: Basic principles and recent advances. *Small* **2017**, *13*, 1701931. [[CrossRef](#)] [[PubMed](#)]
15. Lyons, M.E.; Brandon, M.P. The oxygen evolution reaction on passive oxide covered transition metal electrodes in alkaline solution. Part III–Iron. *Int. J. Electrochem. Sci.* **2008**, *3*, 1463–1503.
16. Lyons, M.E.; Brandon, M.P. The oxygen evolution reaction on passive oxide covered transition metal electrodes in alkaline solution part II–cobalt. *Int. J. Electrochem. Sci.* **2008**, *3*, 1425–1462.
17. Lyons, M.E.; Brandon, M.P. The oxygen evolution reaction on passive oxide covered transition metal electrodes in aqueous alkaline solution. Part 1–Nickel. *Int. J. Electrochem. Sci.* **2008**, *3*, 1386–1424.
18. Subbaraman, R.; Tripkovic, D.; Chang, K.; Strmcnik, D.; Paulikas, A.P.; Hirunsit, P.; Chan, M.; Greeley, J.; Stamenkovic, V.; Markovic, N.M. Trends in activity for the water electrolyser reactions on 3 d M (Ni, Co, Fe, Mn) hydr (oxy) oxide catalysts. *Nat. Mater.* **2012**, *11*, 550–557. [[CrossRef](#)]
19. Trotochaud, L.; Ranney, J.K.; Williams, K.N.; Boettcher, S.W. Solution-cast metal oxide thin film electrocatalysts for oxygen evolution. *J. Am. Chem. Soc.* **2012**, *134*, 17253–17261. [[CrossRef](#)]
20. Lyons, M.E.; Brandon, M.P. A comparative study of the oxygen evolution reaction on oxidised nickel, cobalt and iron electrodes in base. *J. Electroanal. Chem.* **2010**, *641*, 119–130. [[CrossRef](#)]
21. Li, X.; Walsh, F.C.; Pletcher, D. Nickel based electrocatalysts for oxygen evolution in high current density, alkaline water electrolyzers. *Phys. Chem. Chem. Phys.* **2011**, *13*, 1162–1167. [[CrossRef](#)] [[PubMed](#)]
22. Oliva, P.; Leonardi, J.; Laurent, J.; Delmas, C.; Braconnier, J.; Figlarz, M.; Fievet, F.; De Guibert, A. Review of the structure and the electrochemistry of nickel hydroxides and oxy-hydroxides. *J. Power Sources* **1982**, *8*, 229–255. [[CrossRef](#)]
23. Diaz-Morales, O.; Ledezma-Yanez, I.; Koper, M.T.; Calle-Vallejo, F. Guidelines for the rational design of Ni-based double hydroxide electrocatalysts for the oxygen evolution reaction. *ACS Catal.* **2015**, *5*, 5380–5387. [[CrossRef](#)]
24. Wang, P.; Lin, Y.; Wan, L.; Wang, B. Autologous growth of Fe-doped Ni(OH)<sub>2</sub> nanosheets with low overpotential for oxygen evolution reaction. *Int. J. Hydrog. Energy* **2020**, *45*, 6416–6424. [[CrossRef](#)]
25. Suib, S.L. *New and Future Developments in Catalysis: Hybrid Materials, Composites, and Organocatalysts*; Newnes: London, UK, 2013.
26. Cordoba, S.; Carbonio, R.; Teijelo, M.L.; Macagno, V. The electrochemical response of binary mixtures of hydrous transition metal hydroxides co-precipitated on conducting substrates with reference to the oxygen evolution reaction. *Electrochim. Acta* **1986**, *31*, 1321–1332. [[CrossRef](#)]
27. Corrigan, D.A. The catalysis of the oxygen evolution reaction by iron impurities in thin film nickel oxide electrodes. *J. Electrochem. Soc.* **1987**, *134*, 377. [[CrossRef](#)]
28. Stevens, M.B.; Enman, L.J.; Korkus, E.H.; Zaffran, J.; Trang, C.D.; Asbury, J.; Kast, M.G.; Toroker, M.C.; Boettcher, S.W. Ternary Ni-Co-Fe oxyhydroxide oxygen evolution catalysts: Intrinsic activity trends, electrical conductivity, and electronic band structure. *Nano Res.* **2019**, *12*, 2288–2295. [[CrossRef](#)]

29. Pavel, C.C.; Cecconi, F.; Emiliani, C.; Santuccioli, S.; Scaffidi, A.; Catanorchi, S.; Comotti, M. Highly efficient platinum group metal free based membrane-electrode assembly for anion exchange membrane water electrolysis. *Angew. Chem. Int. Ed.* **2014**, *53*, 1378–1381. [[CrossRef](#)]
30. Leng, Y.; Chen, G.; Mendoza, A.J.; Tighe, T.B.; Hickner, M.A.; Wang, C. Solid-state water electrolysis with an alkaline membrane. *J. Am. Chem. Soc.* **2012**, *134*, 9054–9057. [[CrossRef](#)]
31. Parrondo, J.; Arges, C.G.; Niedzwiecki, M.; Anderson, E.B.; Ayers, K.E.; Ramani, V. Degradation of anion exchange membranes used for hydrogen production by ultrapure water electrolysis. *Rsc. Adv.* **2014**, *4*, 9875–9879. [[CrossRef](#)]
32. Zeng, L.; Zhao, T. Integrated inorganic membrane electrode assembly with layered double hydroxides as ionic conductors for anion exchange membrane water electrolysis. *Nano Energy* **2015**, *11*, 110–118. [[CrossRef](#)]
33. Bates, M.K.; Jia, Q.; Doan, H.; Liang, W.; Mukerjee, S. Charge-transfer effects in Ni–Fe and Ni–Fe–Co mixed-metal oxides for the alkaline oxygen evolution reaction. *ACS Catal.* **2016**, *6*, 155–161. [[CrossRef](#)]
34. Trotochaud, L.; Young, S.L.; Ranney, J.K.; Boettcher, S.W. Nickel–iron oxyhydroxide oxygen-evolution electrocatalysts: The role of intentional and incidental iron incorporation. *J. Am. Chem. Soc.* **2014**, *136*, 6744–6753. [[CrossRef](#)]
35. Gong, M.; Li, Y.; Wang, H.; Liang, Y.; Wu, J.Z.; Zhou, J.; Wang, J.; Regier, T.; Wei, F.; Dai, H. An advanced Ni–Fe layered double hydroxide electrocatalyst for water oxidation. *J. Am. Chem. Soc.* **2013**, *135*, 8452–8455. [[CrossRef](#)] [[PubMed](#)]
36. Li, Y.; Selloni, A. Mechanism and activity of water oxidation on selected surfaces of pure and Fe-doped NiO<sub>x</sub>. *ACS Catal.* **2014**, *4*, 1148–1153. [[CrossRef](#)]
37. Bo, X.; Li, Y.; Hocking, R.K.; Zhao, C. NiFeCr hydroxide holey nanosheet as advanced electrocatalyst for water oxidation. *ACS Appl. Mater. Interfaces* **2017**, *9*, 41239–41245. [[CrossRef](#)]
38. Jin, Y.; Huang, S.; Yue, X.; Du, H.; Shen, P.K. Mo- and Fe-modified Ni(OH)<sub>2</sub>/NiOOH nanosheets as highly active and stable electrocatalysts for oxygen evolution reaction. *ACS Catal.* **2018**, *8*, 2359–2363. [[CrossRef](#)]
39. Dinh, K.N.; Zheng, P.; Dai, Z.; Zhang, Y.; Dangol, R.; Zheng, Y.; Li, B.; Zong, Y.; Yan, Q. Ultrathin porous NiFeV ternary layer hydroxide nanosheets as a highly efficient bifunctional electrocatalyst for overall water splitting. *Small* **2018**, *14*, 1703257. [[CrossRef](#)]
40. Cossar, E.; Barnett, A.O.; Seland, F.; Safari, R.; Botton, G.A.; Baranova, E.A. Ionomer content optimization in nickel-iron-based anodes with and without ceria for anion exchange membrane water electrolysis. *J. Power Sources* **2021**, *514*, 230563. [[CrossRef](#)]
41. López-Fernández, E.; Gómez-Sacedón, C.; Gil-Rostra, J.; Espinós, J.; González-Elipe, A.; Yubero, F.; de Lucas-Consuegra, A. Ionomer-Free Nickel-Iron bimetallic electrodes for efficient anion exchange membrane water electrolysis. *Chem. Eng. J.* **2021**, *433*, 133774. [[CrossRef](#)]
42. Xu, D.; Stevens, M.B.; Cosby, M.R.; Oener, S.Z.; Smith, A.M.; Enman, L.J.; Ayers, K.E.; Capuano, C.B.; Renner, J.N.; Danilovic, N. Earth-abundant oxygen electrocatalysts for alkaline anion-exchange-membrane water electrolysis: Effects of catalyst conductivity and comparison with performance in three-electrode cells. *ACS Catal.* **2018**, *9*, 7–15. [[CrossRef](#)]
43. Kang, Z.; Yu, S.; Yang, G.; Li, Y.; Bender, G.; Pivovar, B.S.; Green Jr, J.B.; Zhang, F. Performance improvement of proton exchange membrane electrolyzer cells by introducing in-plane transport enhancement layers. *Electrochim. Acta* **2019**, *316*, 43–51. [[CrossRef](#)]
44. Vincent, I.; Lee, E.; Kim, H. Comprehensive impedance investigation of low-cost anion exchange membrane electrolysis for large-scale hydrogen production. *Sci. Rep.* **2021**, *11*, 293. [[CrossRef](#)] [[PubMed](#)]
45. Yang, G.; Mo, J.; Kang, Z.; Dohrmann, Y.; List, F.A., III; Green, J.B., Jr.; Babu, S.S.; Zhang, F. Fully printed and integrated electrolyzer cells with additive manufacturing for high-efficiency water splitting. *Appl. Energy* **2018**, *215*, 202–210. [[CrossRef](#)]
46. Han, B.; Mo, J.; Kang, Z.; Zhang, F. Effects of membrane electrode assembly properties on two-phase transport and performance in proton exchange membrane electrolyzer cells. *Electrochim. Acta* **2016**, *188*, 317–326. [[CrossRef](#)]
47. Ge, J.; Higier, A.; Liu, H. Effect of gas diffusion layer compression on PEM fuel cell performance. *J. Power Sources* **2006**, *159*, 922–927. [[CrossRef](#)]
48. Li, D.; Motz, A.R.; Bae, C.; Fujimoto, C.; Yang, G.; Zhang, F.; Ayers, K.E.; Kim, Y.S. Durability of anion exchange membrane water electrolyzers. *Energy Environ. Sci.* **2021**, *14*, 3393–3419. [[CrossRef](#)]
49. Pham, T.H.; Olsson, J.S.; Jannasch, P. Poly (arylene alkylene)s with pendant N-spirocyclic quaternary ammonium cations for anion exchange membranes. *J. Mater. Chem. A* **2018**, *6*, 16537–16547. [[CrossRef](#)]
50. Olsson, J.S.; Pham, T.H.; Jannasch, P. Poly (arylene piperidinium) hydroxide ion exchange membranes: Synthesis, alkaline stability, and conductivity. *Adv. Funct. Mater.* **2018**, *28*, 1702758. [[CrossRef](#)]
51. Liu, Z.; Sajjad, S.D.; Gao, Y.; Yang, H.; Kaczur, J.J.; Masel, R.I. The effect of membrane on an alkaline water electrolyzer. *Int. J. Hydrog. Energy* **2017**, *42*, 29661–29665. [[CrossRef](#)]
52. Henkensmeier, D.; Najibah, M.; Harms, C.; Žitka, J.; Hnát, J.; Bouzek, K. Overview: State-of-the art commercial membranes for anion exchange membrane water electrolysis. *J. Electrochem. Energy Convers. Storage* **2021**, *18*, 024001. [[CrossRef](#)]
53. Ayers, K.; Danilovic, N.; Ouimet, R.; Carmo, M.; Pivovar, B.; Bornstein, M. Perspectives on low-temperature electrolysis and potential for renewable hydrogen at scale. *Annu. Rev. Chem. Biomol. Eng.* **2019**, *10*, 219–239. [[CrossRef](#)] [[PubMed](#)]
54. Price, S.; Ren, X.; Savage, A.; Beyer, F. Synthesis and characterization of anion-exchange membranes based on hydrogenated poly (norbornene). *Polym. Chem.* **2017**, *8*, 5708–5717. [[CrossRef](#)]
55. Truong, V.M.; Duong, N.B.; Yang, H. Comparison of Carbon Supports in Anion Exchange Membrane Fuel Cells. *Materials* **2020**, *13*, 5370. [[CrossRef](#)]

56. Razmjooei, F.; Reißner, R.; Gago, A.S.; Ansar, A. Highly active binder free plasma sprayed non-noble metal electrodes for anion exchange membrane electrolysis at different reduced KOH concentrations. *ECS Trans.* **2019**, *92*, 689. [[CrossRef](#)]
57. López-Fernández, E.; Sacedón, C.G.; Gil-Rostra, J.; Yubero, F.; González-Elipe, A.R.; de Lucas-Consuegra, A. Recent Advances in Alkaline Exchange Membrane Water Electrolysis and Electrode Manufacturing. *Molecules* **2021**, *26*, 6326. [[CrossRef](#)]
58. Masel, R.I.; Liu, Z.; Sajjad, S. Anion exchange membrane electrolyzers showing 1 A/cm<sup>2</sup> at less than 2 V. *ECS Trans.* **2016**, *75*, 1143. [[CrossRef](#)]
59. Lim, A.; Kim, H.; Henkensmeier, D.; Yoo, S.J.; Kim, J.Y.; Lee, S.Y.; Sung, Y.; Jang, J.H.; Park, H.S. A study on electrode fabrication and operation variables affecting the performance of anion exchange membrane water electrolysis. *J. Ind. Eng. Chem.* **2019**, *76*, 410–418. [[CrossRef](#)]
60. Carbone, A.; Zignani, S.C.; Gatto, I.; Trocino, S.; Aricò, A. Assessment of the FAA3-50 polymer electrolyte in combination with a NiMn<sub>2</sub>O<sub>4</sub> anode catalyst for anion exchange membrane water electrolysis. *Int. J. Hydrog. Energy* **2020**, *45*, 9285–9292. [[CrossRef](#)]
61. Kutz, R.B.; Chen, Q.; Yang, H.; Sajjad, S.D.; Liu, Z.; Masel, I.R. Sustainion imidazolium-functionalized polymers for carbon dioxide electrolysis. *Energy Technol.* **2017**, *5*, 929–936. [[CrossRef](#)]
62. Kaczur, J.J.; Yang, H.; Liu, Z.; Sajjad, S.D.; Masel, R.I. Carbon dioxide and water electrolysis using new alkaline stable anion membranes. *Front. Chem.* **2018**, *6*, 263. [[CrossRef](#)] [[PubMed](#)]
63. Pushkareva, I.; Pushkarev, A.; Grigoriev, S.; Modisha, P.; Bessarabov, D. Comparative study of anion exchange membranes for low-cost water electrolysis. *Int. J. Hydrog. Energy* **2020**, *45*, 26070–26079. [[CrossRef](#)]